

# Structural Properties of Mn Doped ZnO Nanocrystallites Using Wet Chemical Synthesis

Nii Abekah Akwetey Armah<sup>1, 2</sup>, Hubert Azoda Koffi<sup>1\*</sup>

<sup>1</sup> Department of Physics, University of Ghana, Legon, LG 63, Accra, Ghana

<sup>2</sup> Foundation Department, Lancaster University Ghana, P. O. Box CT9823, Cantonments, Accra, Ghana

\* Corresponding author email: hakoff@ug.edu.gh / hazokoff@gmail.com

Received: 12-05-2023, Received in Revised form: 15-06-2023, Accepted: 15-06-2023, Published: 30-06-2023

## Abstract

To get the required electrical, magnetic, structural and optical properties, materials are required to be doped with suitable impurities. The use of transition metals as a dopant in ZnO has been investigated to determine how they alter the various properties. Several research concerning the synthesis of TM-doped ZnO via various methods with the solubility limit of TM elements in ZnO has been reported. The distribution of the TMs into the ZnO matrix has been reported with divergent views. In this work, Mn doped ZnO nanoparticles has been synthesized by means of reasonable and ecologically friendly procedure by means of the liquid phase method with fewer conservational contaminants and no leftover products. The influence of the dopant on the structural properties of the produced ZnO nanocrystals was scrutinized using powder x-ray diffractogram (XRD). The Mn-doping concentration,  $x$ , was varied ( $0.05 \leq x \leq 0.5$ ) at temperatures of 180°C and 200 °C. Results of the lattice parameters, bond length, bond angles, crystallite size, strain, volume of unit cell, APF, number of unit cells, specific surface area and the density of the Mn-doped ZnO nanocrystal samples were be irregular in nature and not following a particular trend as the doping concentration increases. This variation in the values were due to the irregular values of the interplanar spacing and the observed variations in the shift of the peak angles as a result of the difference in ionic radii between Zn and Mn ions with Mn having multiple ionic radii since all the parameters are directly dependent on the value of the  $2\theta$ .

**Keywords:** Nanocrystals, ZnO, Mn-doping, Concentration, Temperature, Structural.

## Background Introduction

In scientific and industrial applications, the richest classes of materials among the wide range according to properties such as physical, chemical, and structural are the metal oxides which happen to be probably the most common due to the abundancy of oxygen, especially the TCO (transparent conducting oxides) materials. In the group of metal oxides, the transition metals are able to form several oxide phases with ions in diverse oxidation states. Within this group, the properties depend vehemently on the type of ionic metal due to changes resulting from characteristic of the interactions of ionic-covalent bonding. The relation between the ionic radii sizes and structure properties becomes the most significant issue [1].

Among the transition metals, ZnO in particular have attracted increasing attention recently as a replacing material for ITO for the reason that, it is bountiful, low-priced and primarily non-toxicity of Zn. As a result, improving ZnO with alternative impurity dopants stands out as the best potential alternative candidate for ITO [2][3]. To get the required electrical, magnetic, structural and optical properties, TCO materials are required to be doped with suitable impurities. Semiconducting materials exhibit ferromagnetic properties at and above room temperature when doped with transition-metal (TM) cations such as Mn, Cr, Fe, Co, and Ni. These transition-metal doped semiconductors are called dilute magnetic semiconductors (DMS's) [4].

The DMS's aim to utilize the spin properties by injecting a magnetic ion into conventional semiconductors to generate spin-polarized currents. The spin properties, brought into been the fundamental idea of spintronic. Spintronic devices function by generating spin-polarized currents and its applications are found in bionics, for accurate perception of touch, sound, and vision, and enable neuromorphic computing to create faster processors that resolve accuracy issues in several areas of studies such as defects and disorders in

materials, metrology, and space exploration [4]. As a result, research into such materials has been on the increase in the past decade.

Among the many transition metal oxides, and out of all the 3d metal ions dopants, manganese as an element is biocompatible and manganese oxide is the only binary compound that parades a diversity of oxidation states ensuing in assorted chemical and structural formulae such as MnO, MnO<sub>2</sub>, Mn<sub>2</sub>O<sub>3</sub>, Mn<sub>3</sub>O<sub>4</sub>, and Mn<sub>5</sub>O<sub>8</sub> forms [5]. It also has multiple ionic radii which makes the chemistry of its compounds very rich. Also, Mn is preferred because the energy level of its d electron can easily overlap with the valence band of ZnO which subsequently affects the physical, chemical and structural properties of the host [6].

Mn-doped ZnO nanoparticles become awfully a dynamic material for its co-existing magnetic, semiconducting and optical properties [7]. It has also increased a lot of attention due to its numerous applications including photocatalyst, chemical sensors, solar cells, optoelectronic, biological, medical devices, etc. [8][9]. Due to vast interest, it is of great importance to explore the relationship between the local environment around Mn and the magnetic properties, electronic structure, and optical properties of the Mn-doped ZnO nanoparticles [10].

Several research concerning the synthesis of TM-doped ZnO via various methods with the solubility limit of TM elements in ZnO has reported the distribution of the TMs into the ZnO matrix with divergent views. Results of researchs on Mn-doped ZnO nanoparticles produced for the past ten years has also been reported with quite a lot of possible results. Experimental data reviewed so far have suggested that, increasing Mn-dopant concentration in the synthesis of ZnO nanoparticles can yield a resultant variation (either increase or decrease) in the structural and optical properties.

Some publications have observed a shift in the XRD peaks with Mn doping concentration with comparison of ZnO phases and attributed it to the change in the ionic radii of Mn and Zn.

<https://doi.org/10.24949/njes.v16i1.756>



Most of these shifts has been reported to shift negatively or towards lower angles (shifted to a lower  $2\theta$  value). In addition, the width of the peak is found to vary with rise in concentration of dopant [4] [6] [11]. Similarly, it has also been reported that, introduction of manganese ions shifts the diffraction peaks to higher angles [9]. The disagreements arise, at least in part, from incomplete characterization of the system in terms of structural properties and crystallinity. It has also been suggested that increasing the synthesis condition such as temperature can also alter these properties.

However, based on the previous work of Armah et al [5], it was observed that there were swings in peak locations in the diffraction pattern because of increasing Mn concentration and temperature which were irregular (increase and decrease). As a result, the need to investigate first into the structural and subsequently the optical properties to determine the effect of this irregular variation. Therefore, the specific goal of this research is to explore the effect of the variation of doping concentration on the structural properties such as lattice parameters, positional parameter, bond length, bond angles, crystallite size, dislocation density, lattice strain, unit cell volume, APF, number of unit cells, specific surface area and the density of the samples using powder X-ray diffractometer (XRD).

### Experimental Procedures

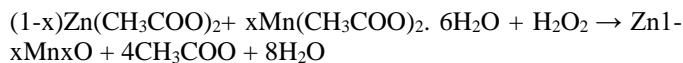
The chemicals used in the production of the samples for this research investigation are given below. The chemicals were attained from Maalab Scientific Equipment PVT, Ltd, Madhura Nagar, India.

- Hydrogen Peroxide, 30%
- Methanol, 99%
- Zinc acetate dehydrate, 98.50%
- Manganese acetate tetrahydrate, 99%

### Sample Preparation

The Mn-doped ZnO nanoparticles were synthesized using a simple wet chemical which was reported in our previous work [5]. In the doping procedure, a suitable amount of metal precursors depending on the doping concentrations, were ground in an agate mortar and transferred into a beaker holding an amount of methanol. The beaker was placed in a sonicator for roughly 10 mins and later transferred to a hot plate at temperature range between 50 and 65 °C. As the solution was being sonicated, trickles of hydrogen peroxide were added using a syringe. The resulting solution showing brownish colour was heated at temperatures between 100 °C and 120 °C until all the solution evaporated and the product solidified into crystals. The brownish crystals after cooling were grounded and returned back to the hot plate at starting temperature of 120 °C which was gradually increased to 180 °C within a time of 20 minutes and maintained there for about one hour. The doping concentration,  $x$ , was varied as ( $0.05 < x < 0.5$ ). Diagram displaying the manganese doped ZnO nanoparticles synthesis procedure is shown in figure 1.

The entire process was repeated and the thermal decomposition temperature varied by increasing to 200°C. The reaction taking place throughout synthesis process is as displayed below:



During the synthesis process, a colour change was observed from ash to brown when the manganese acetate salts were added to the zinc acetate solution. The colors became more intense with higher dopant concentrations. The temperature and time used during the doping process for the acetates to dissolve was found to increase as dopant concentration increased.

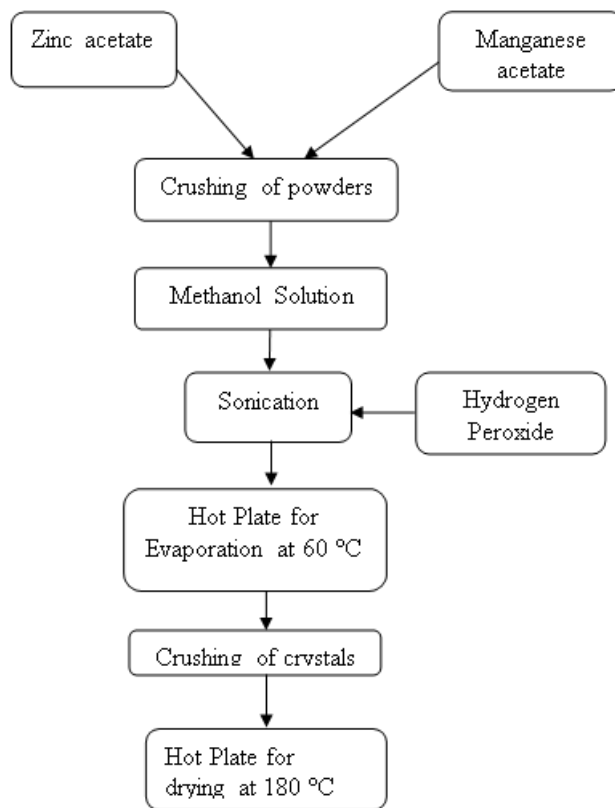


Figure 1: Diagram Showing the Synthesis of the Mn Doped ZnO

### Structural Characterization

For the structural characterization, using an X-ray powder diffractometer (PANalytical) as described earlier by Armah et al [5] and Armah and Azoda [12], the following parameters were determined using the appropriate formulae. Equation 1 was used to estimate the values of the lattice parameters  $a$  and  $c$  [13][14]:

$$\frac{1}{d^2} = \frac{4}{3} \left[ \frac{h^2 + hk + k^2}{a^2} \right] + \frac{l^2}{c^2} \quad (1)$$

The positional or internal parameter,  $u$ , and the Zn—O bond lengths of that along the  $c$ -direction,  $b$ , and that off the  $c$ -axis (expressed as  $b_1 = L$ ) were determined using equations (2) [15][16], (3) and (4) [12][17][18] respectively:

$$u = \frac{a^2}{3(c)^2} + 0.25 \quad (2)$$

$$b = cu \quad (3)$$

$$b_1 = L = \sqrt{\frac{1}{3}a^2 + \left(\frac{1}{2} - u\right)^2 c^2} \quad (4)$$

The respective bond angles,  $\alpha$  and  $\beta$ , are given by the equations (5) and (6) [12][18][19]:

$$\alpha = \frac{\pi}{2} + \arccos \left[ \left( \sqrt{1 + 3 \left( \frac{c}{a} \right)^2 \left( -u + \frac{1}{2} \right)^2} \right)^{-1} \right] \quad (5)$$

$$\beta = 2 \arcsin \left[ \left( \sqrt{\frac{4}{3} + 4 \left( \frac{c}{a} \right)^2 \left( -u + \frac{1}{2} \right)^2} \right)^{-1} \right] \quad (6)$$

The Debye- Scherrer equation (7) was used to calculate the average crystallite size,  $D$  in nm, [14][15] were as equations (8) and (9) were used to calculate the dislocation density ( $\delta$ ) [20][21] and the Lattice strain,  $\epsilon$ , [21][22] respectively:

$$D = \frac{k\lambda}{\beta \cos \theta} \quad (7)$$

$$\delta = \frac{1}{D^2} \quad (8)$$

$$\epsilon = \frac{\beta}{4 \tan \theta} \quad (9)$$

where  $\lambda$  is the X-ray wavelength in nm,  $k$  is a constant with value of 0.9,  $\theta$  is the Bragg's angle in radians, and  $\beta$  is the full width at half maximum of the peak in radians.

The ideal volume of the unit cell,  $V$ , which is equal to the area of the base of the unit cell multiplied by the height of the unit cell, the number of unit cells ( $n$ ) and the Atomic packing fraction (APF) were obtained from the equations (10) [22][23], (11) [12][24] and (12) [15][22] respectively:

$$V = \frac{\sqrt{3}}{2} a^2 c = 0.866 a^2 c \quad (10)$$

$$n = \frac{4}{3} \pi \left( \frac{D}{2} \right)^3 \frac{1}{V} = \frac{\pi D^3}{6V} \quad (11)$$

$$APF = \frac{2\pi}{3\sqrt{3}} \left( \frac{a}{c} \right) \quad (12)$$

The specific surface area ( $S_a$ ) defined as the total surface area of a material per unit of mass can be determining from particle

size of the ZnO nanoparticles using the relation of equation (13) [12][21][25]:

$$S_a = \frac{6 \times 10^3}{\rho \times D} \quad (13)$$

with  $\rho$  being the density of the ZnO which can be calculated by the equation (14) [12]:

$$\rho = \frac{ZM}{N_A V} \quad (14)$$

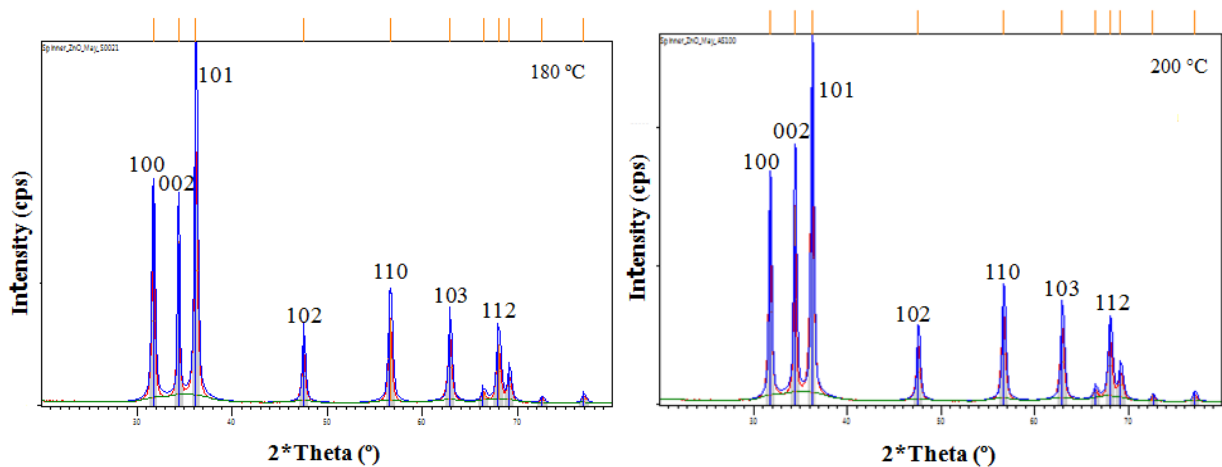
From equations (14)  $Z$  is the number of formula units of ZnO which is 2,  $M$  is molecular weight of ZnO (81.4 g/mol),  $N_A$  is Avogadro's number ( $6.02 \times 10^{23}$ ) and  $V$  is the unit cell volume.

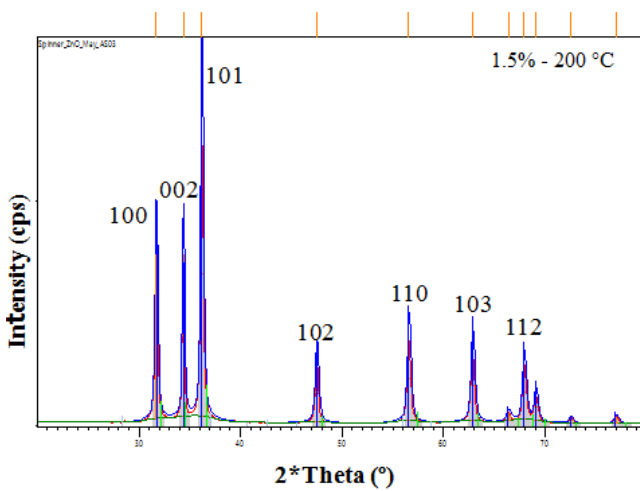
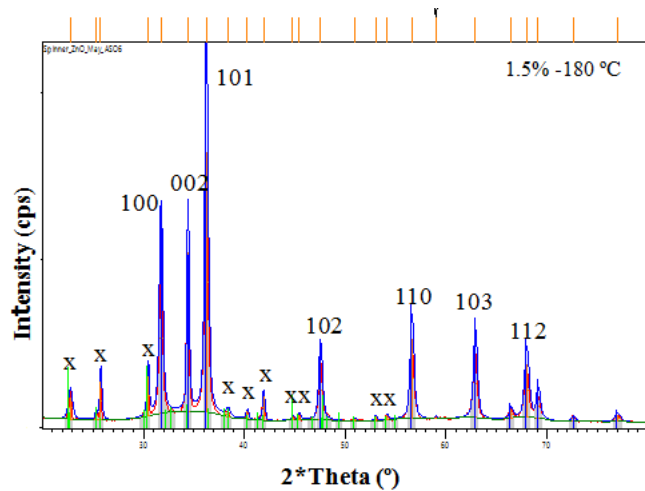
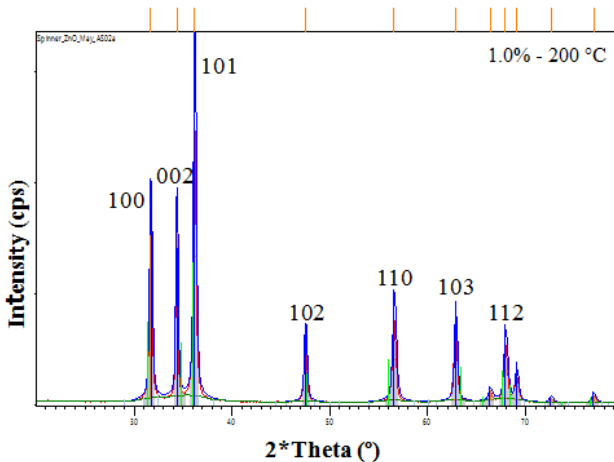
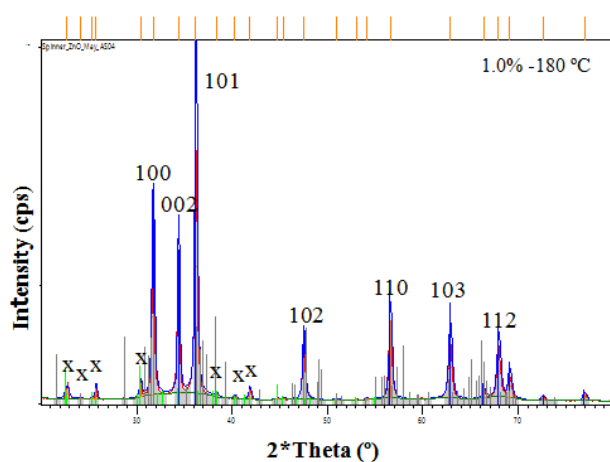
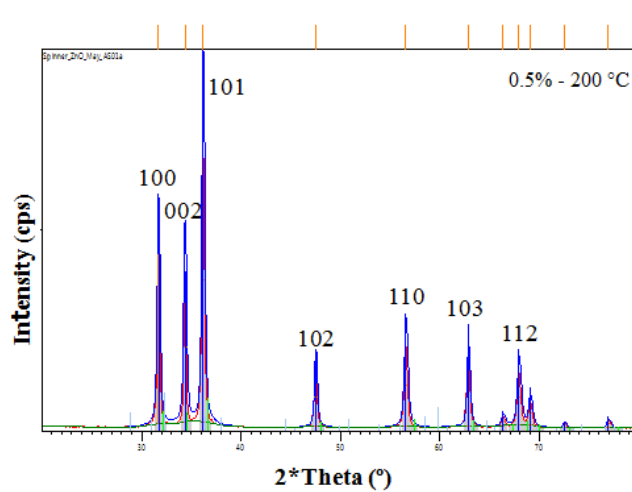
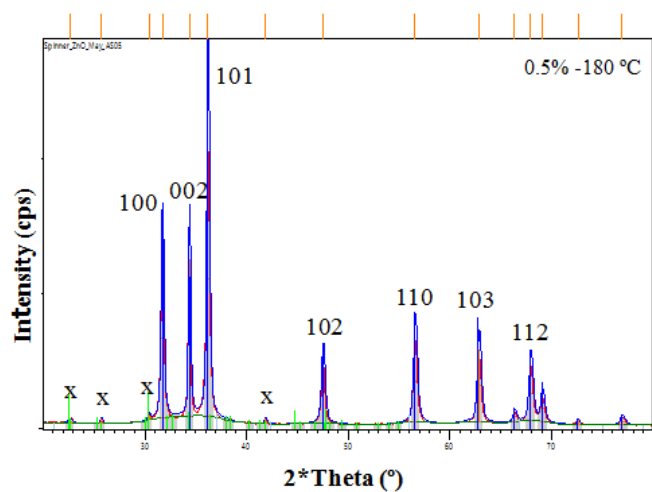
## Results and Discussion

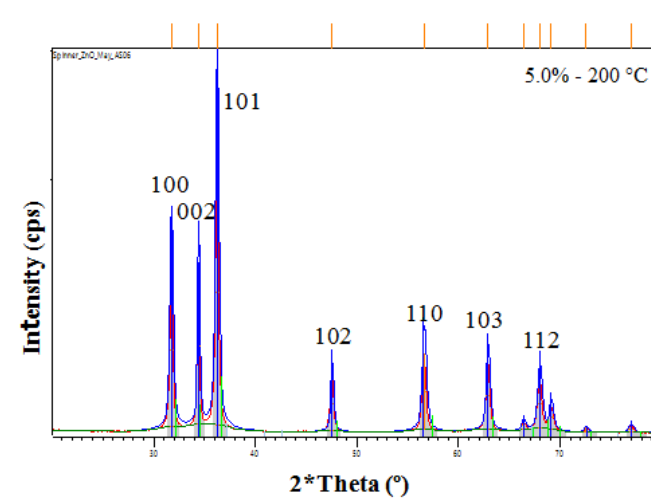
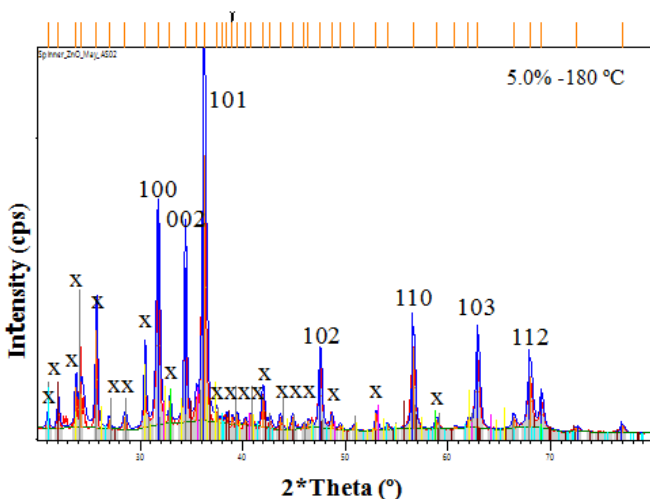
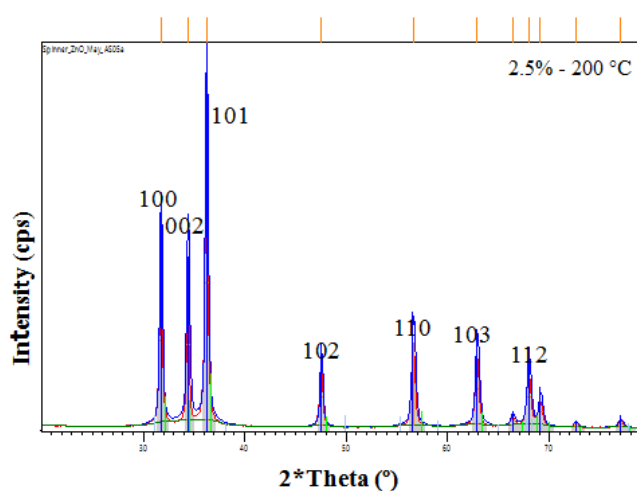
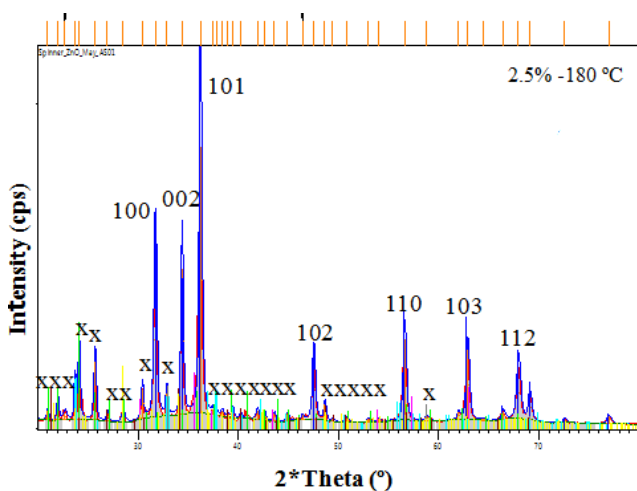
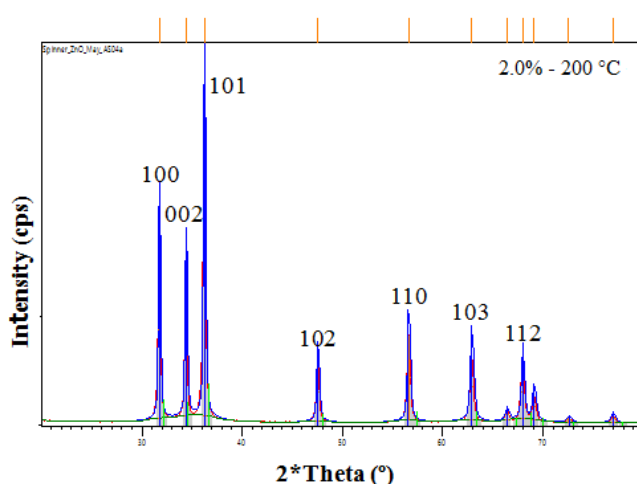
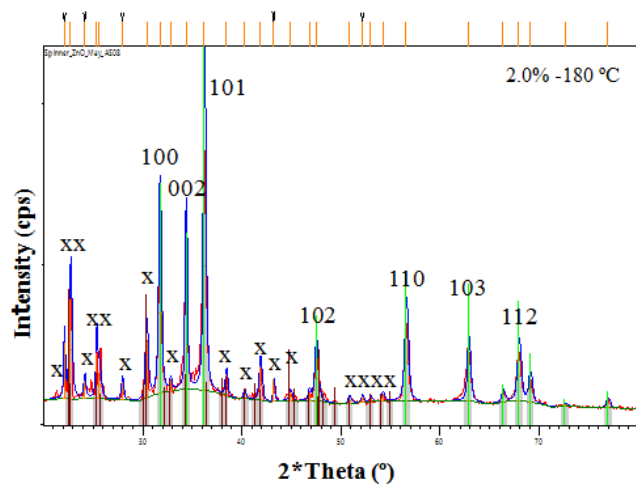
The structural properties considered for investigation as mentioned in structural characterization above includes peak indexing or phase determination, lattice parameters, positional parameter, bond length, bond angles, crystallite size, dislocation density, lattice strain, unit cell volume, APF, number of unit cells, specific surface area and the density of the samples.

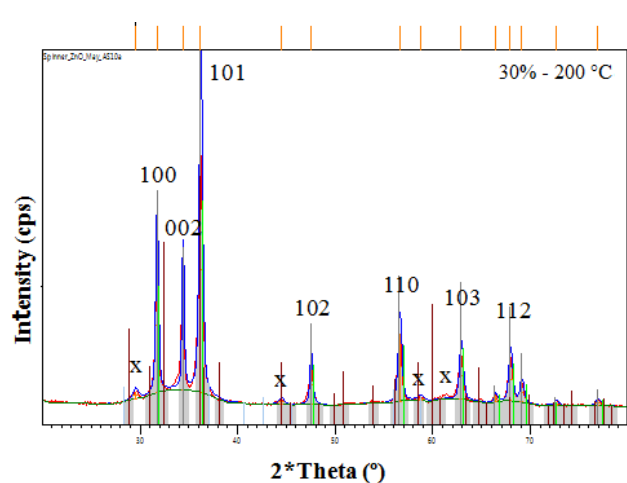
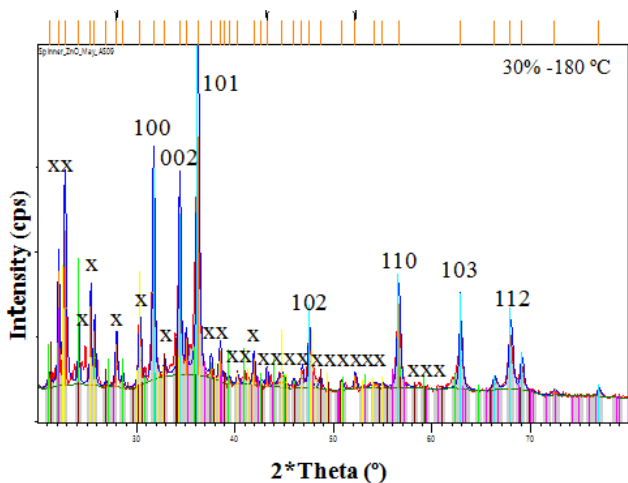
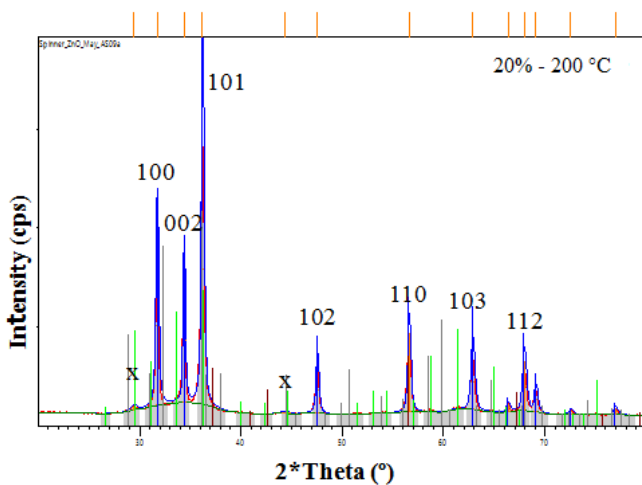
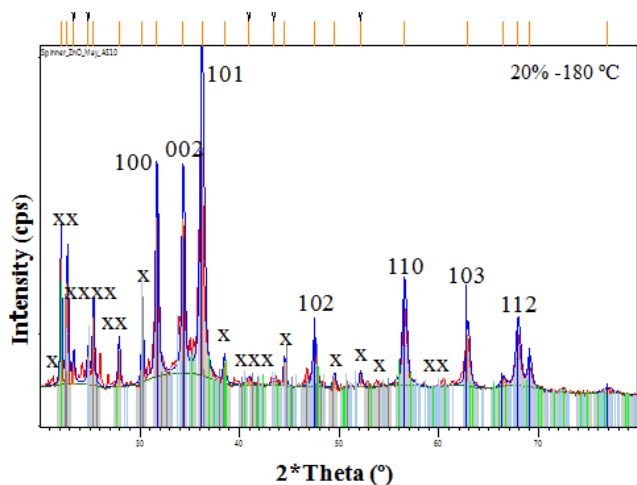
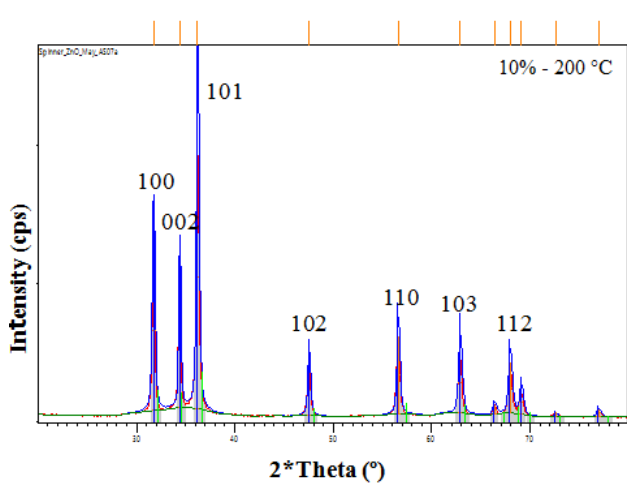
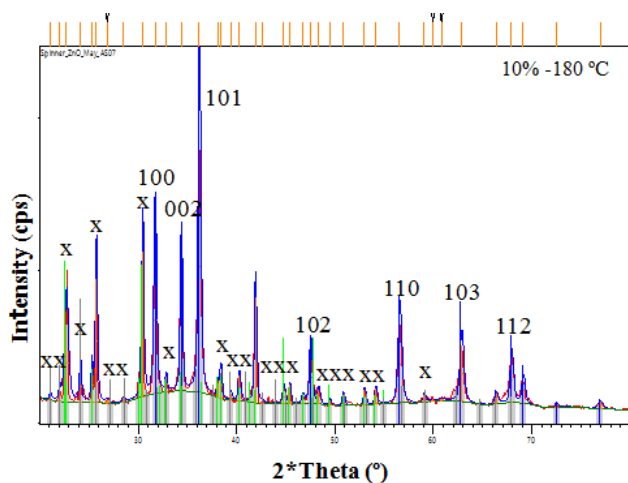
### Peak Positions Indexing

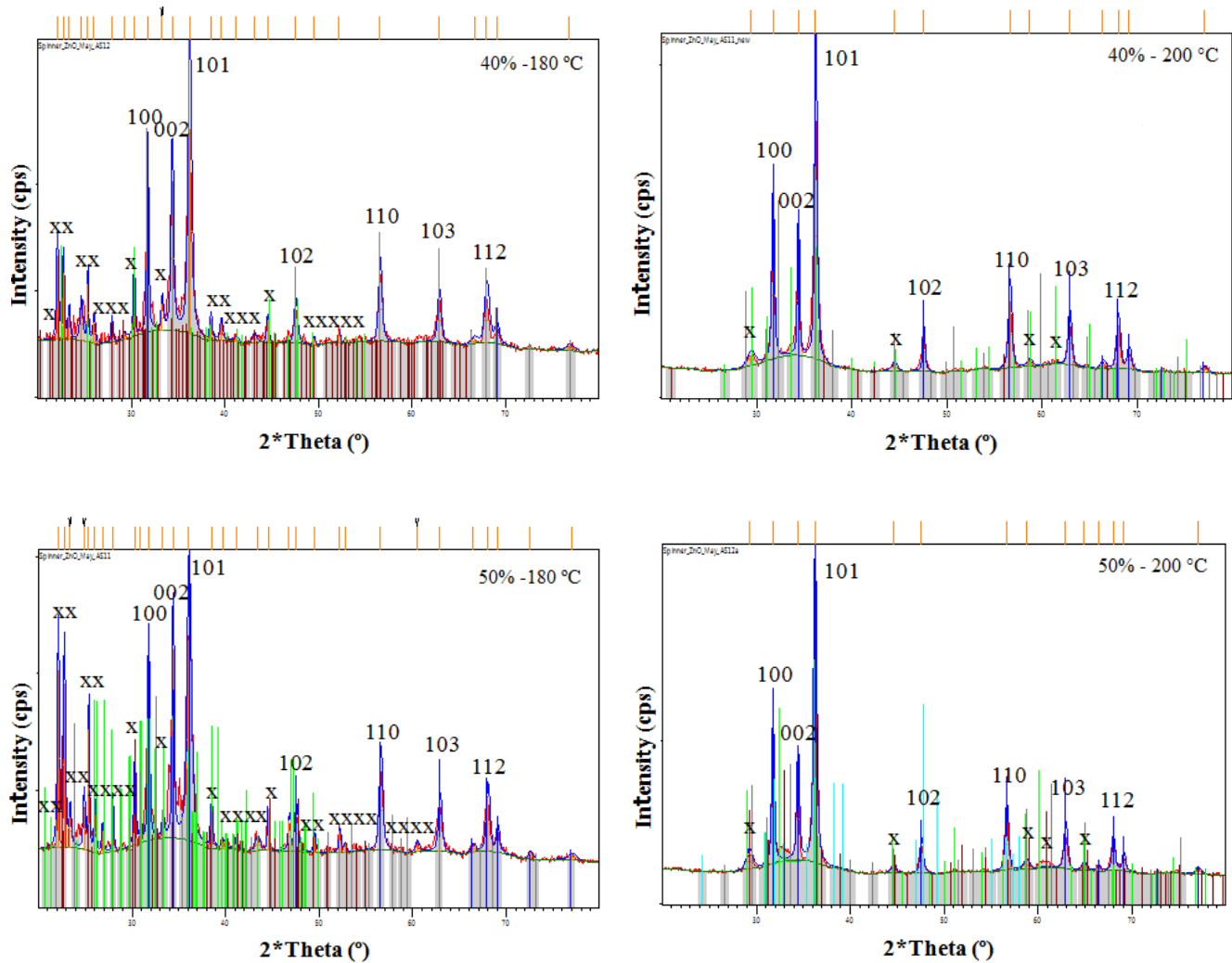
Figure 2 show diffractograms of Mn doped ZnO nanocrystals produced at 180 °C and 200 °C respectively using nominal concentration of doping between 0.5% and 50%. It could be observed from the diffractograms that, as the manganese acetate is introduced, apart from the characteristic peaks index to the (100), (002), (101), (102), (110), (103) and (112), peaks labelled (x) are observed. By increasing the concentration of dopants, the observed peaks labelled "x" and the corresponding intensities also increases







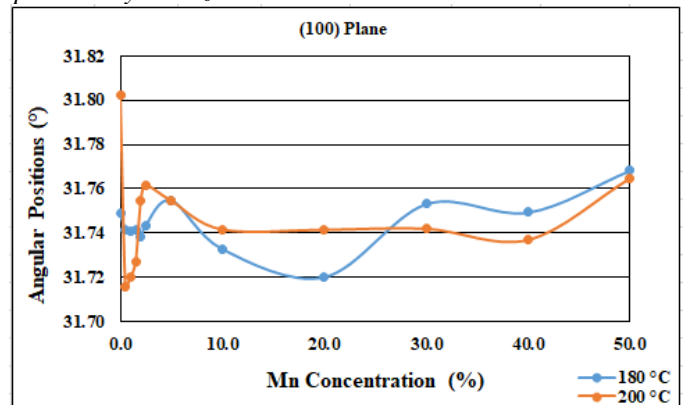




**Figure 2:** Diffractograms of Mn doped ZnO nanoparticles synthesized at 180 °C and 200 °C.

It can be observed that, increasing the temperature from 180 °C to 200 °C, most of these peaks labelled 'x' observed in samples synthesized at 180 °C disappear completely. It has been reported by Armah et al [5] that the low solubility of transition metals in ZnO results in the formation of these secondary phases or additional peaks. The XRD patterns shown above confirm the hexagonal wurtzite structure of ZnO and match very well with the standard data according to ICSD card numbers 01-073-8765 and 01-078-2585 respectively. These peak positions are also very close with JCPDS card no. 36-1451 for ZnO powder. It was also observed that increasing the temperature enables a sharper and narrow peak causing a decrease in their width.

In this work, shifts in peak positions owing to Mn concentration and temperature increment have been detected to be irregular (increasing and decreasing) taking the strongly pronounced or prominent peaks at (100), (002) and (101) planes. The plots in figure 3 below shows the trend of the angular position of the peaks using the (100) and (002) planes respectively.



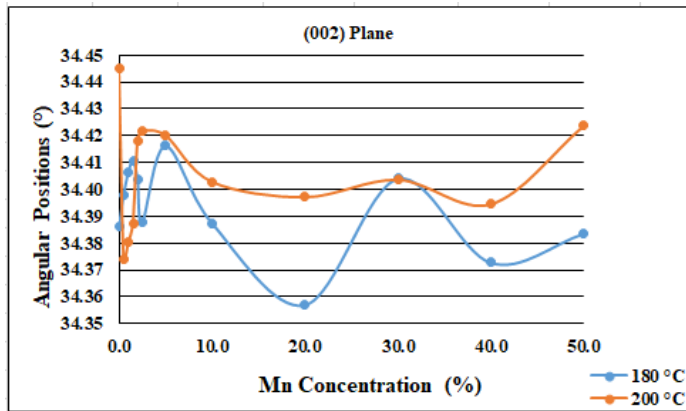


**Figure 3:** The angular Positions as a function of doping concentration at 180 °C and 200 °C

It could be observed that, as temperature increased, generally, there was an upsurge in peak positions causing a drift towards higher diffraction angles. However, as the dopant was introduced into the ZnO, the shift in peak position was irregular (shifting towards both lower and higher diffraction angles). The shifting towards both lower and higher diffraction angles is an indication of the Mn dopant being infused into the lattice of the host, ZnO, and therefore a slight displacement occurs in the crystal dimensions [11][26]. This irregularity leads to the expansion and contraction of the lattice parameters and volume of the unit cell and could be laid at the doorsteps of the method and conditions of preparation of the samples permitting Mn of diverse disseminations into the ZnO edifice [5][27].

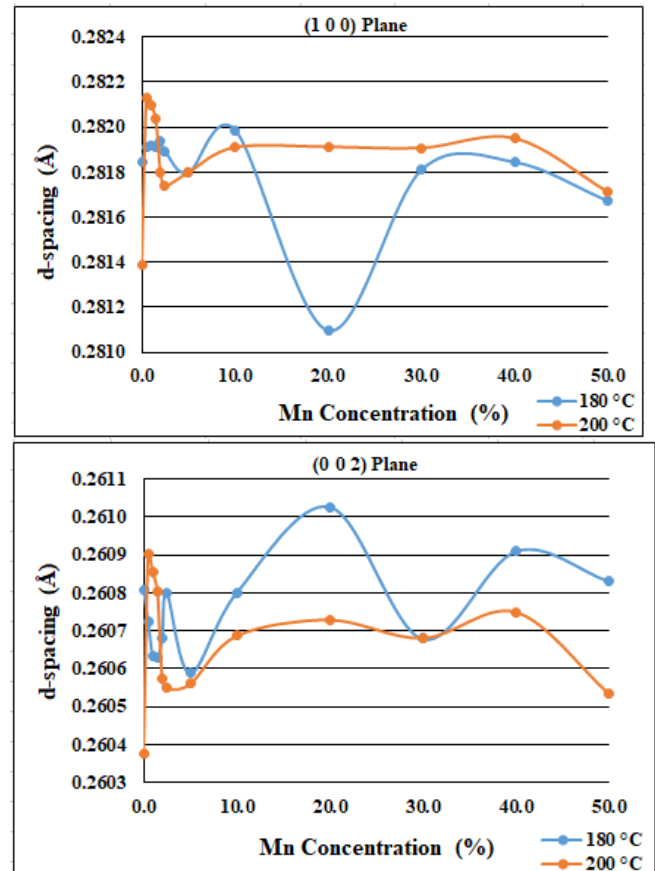
Because  $Zn^{2+}$  (with ionic radius of  $0.74 \text{ \AA}$ ) could be replaced or substituted by  $Mn^{2+}$ ,  $Mn^{3+}$  or  $Mn^{4+}$  (with ionic radii of  $0.83 \text{ \AA}$ ,  $0.65 \text{ \AA}$  and  $0.53 \text{ \AA}$ ) in the lattice, the swaping involves an expansion or contraction of the lattice owing to ionic radii variances [5]. This situation will change the lattice which will result in increasing or decreasing of the interplanar distance (d-spacing). The finding of irregular trend of the  $2\theta$  values has also been reported by Othman et al [15] and Bilgili [22]. Also, the change in angular plane as temperature increases as been reported by Abdulrahman et al [13]).

#### Interplanar Spacing (d-spacing)

It could be observed that, the irregular shift in peak positions also resulted in an irregularity (increasing and decreasing) of the d-spacings for the samples as doping concentration increases and is as shown in figure 4 below for the (100) and (002) planes.

According to Bragg's law, increase in d-spacing causes XRD peaks to shift left (towards lower diffraction angles) while decrease d-spacing causes shift to right (towards higher diffraction angles). It is well known fact that in a perfect crystal, the d-spacings between parallel atomic planes do not change across the whole crystal volume. Nevertheless, in real crystals where there are always possibilities of different kinds of defects, the defects produce deformations which cause local changes of the lattice d-spacings. If the lattice defects are chaotically distributed across the crystal volume, the local d-spacings will fluctuate about some average values. For the dopant in question, swaping Mn family with  $Zn^{2+}$  may cause expansion or contraction of the lattice owing to ionic radii

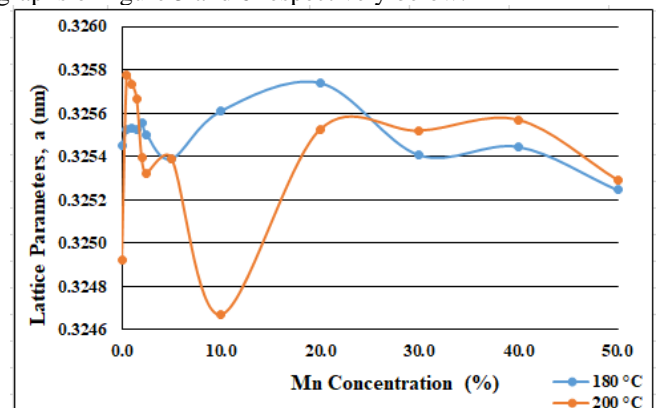
variances. The expansion or contraction by the Mn dopant ions in the host ZnO lattice rather leads to increased static distortion in the crystal structure as reported by [5]. The XRD results show that the sample contained a mixture of different compounds. These are the result of insoluble zinc acetate and its residue in the form of  $Zn(CH_3COO)_2$ ,  $2CH_3COOH$ ,  $2CH_3COO$  and insoluble Mn in the form  $MnO$ ,  $MnO_2$ ,  $Mn_2O_3$ ,  $Mn_3O_4$ , and  $Mn_5O_8$ .



**Figure 4:** The d-spacing as a function of doping concentration at 180 °C and 200 °C

#### Lattice parameters

The trend of the lattice parameters ( $a$ ) and ( $c$ ) as a function of doping concentration at 180 °C and 200 °C, is displayed in the graphs of figure 5 and 6 respectively below.



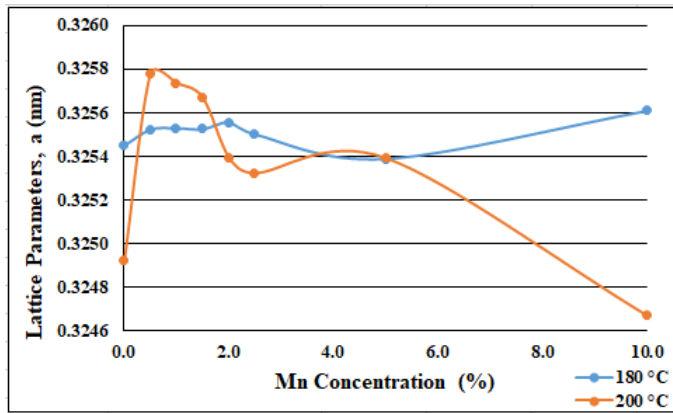


**Figure 5:** The lattice parameter  $a$ , as a function of doping concentration at 180 °C and 200 °C

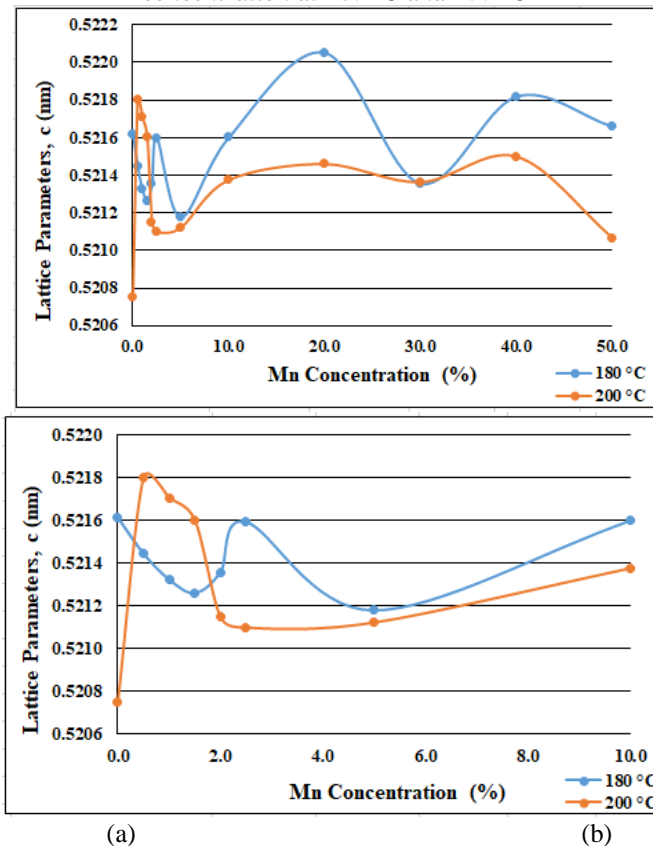


**Figure 6:** The lattice parameter  $c$ , as a function of lower doping concentrations at 180 °C and 200 °C

For the Mn-doped ZnO nanocrystals samples, values at 180 °C were observed to be higher than those of 200 °C. The changes in lattice parameters as temperature increases has been reported by Abdulrahman et al [13]. However, values of the lattice parameters were observed to either increase or decrease as dopant concentration increase without following any trend at both 180 °C and 200 °C respectively.

The maximum values for the lattice parameters ' $a$ ' was found to be at 20% doping concentration at 0.32574 nm for the 180 °C and at 0.5% with corresponding value of 0.32578 nm for the 200 °C. The minimum values are at 50% doping concentrations with corresponding value of 0.32524 nm at both 180 °C and at 10% doping concentrations with

corresponding value of 0.32529 nm at 200 °C respectively (figure 5a). The maximum values for the lattice parameters ' $c$ ' were found to be at 20% and 0.5% doping concentration for both temperatures of 180 °C and 200 °C with corresponding values of 0.52205 nm and 0.52180 nm respectively. The minimum values are at 5% and 50% doping concentrations with corresponding values of 0.52118 nm and for 0.52107 nm respectively (figure 5b).

At higher doping concentrations between 2% and 20%, and between 2% and 50%, the ' $a$ ' and ' $c$ ' values at 180 °C respectively were both found to be higher. From 30% to 50%, the reverse occurs for the ' $a$ ' parameter value. However, at lower doping concentrations between 0.5% and 1.5%, the opposite occurs for both ' $a$ ' and ' $c$ ' where the values at 200 °C were higher.

The upsurge in the lattice parameters ' $a$ ' and ' $c$ ' with respect to doping concentration is due to a smaller ionic radius of Zn than that of  $Mn^{2+}$ . Similarly, the decrease in lattice parameters is caused due to bigger ionic radius of Zn being substituted by  $Mn^{3+}$  and  $Mn^{4+}$  having smaller ionic radii than Zn [28][29]. It can also be caused by zinc vacancies [30]. The length of both ' $a$ ' and ' $c$ ' axis expand and contracts slightly with increasing Mn doping in ZnO. The variation in the lattice parameters with dopant concentration in the crystal can be understood as a phase transition or actual incorporation of dopant into the unit cell of the host structure [29][31].

In addition to the substitution of Mn for Zn in the lattice, interstitial zinc atoms or oxygen vacancies can also be said to have occurred [32]. The lattice parameters of the Mn-doped ZnO nanocrystals that were calculated were found to be independent of composition, within the accuracy of the measurements. Certainly, the lattice parameters of a semiconductor hinge on the concentration of foreign atoms, defects, and the ionic radii differences with veneration to the substituted matrix ions, external strains (e.g., those induced by substrate), and temperature [19]. Similar values of the results have been reported by Othman et al [15] and Belkhaoui et al [16]. However, this irregular trend of the values of the lattice parameters found to be increasing and decreasing as doping concentration increases is similar to preceding reports by Babar [9], Lv et al [11], Abdou and Al-mokhtar [14] and Senol et al [33].

The values of the lattice parameters ( $a$  and  $c$  and their ration  $c/a$ ) obtained for this work has been supported by the report of Belkhaoui et al [16], Nabil et al [20]) and Ara'ujo J'uniol et al [34]. In an ideal wurtzite structure, the  $c/a$  ratio is given 1.633. However, in a real ZnO crystal, the wurtzite structure deviates from the ideal arrangement, by changing the  $c/a$  ratio. The experimentally observed  $c/a$  ratios from this work found to be approximately 1.602 and was smaller than the ideal which is expected as in ideal situation. The deviation from that of the ideal wurtzite crystal is probably due to lattice stability and ionicity [19]. Below is the graph of the ratio  $a/c$  shoing the respective deviations.

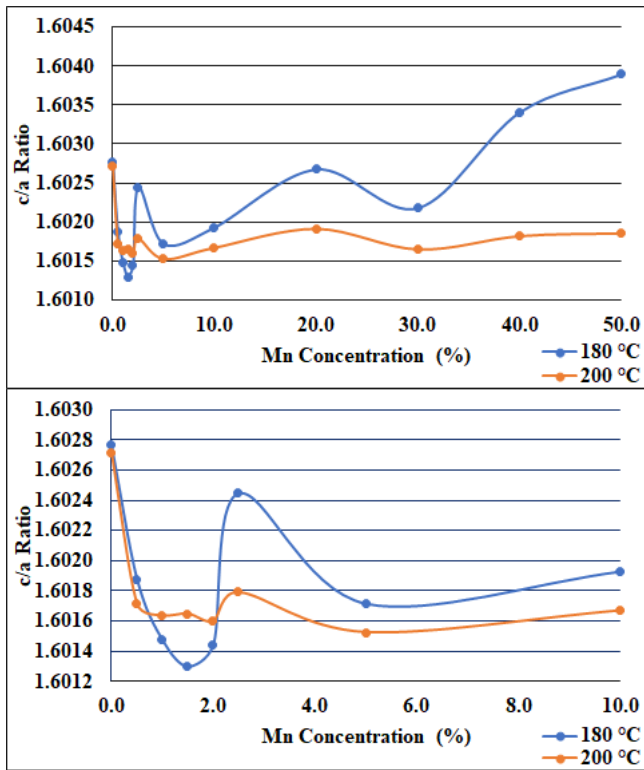


Figure 7: The ratio  $c/a$  as a function of doping concentration at 180 °C and 200 °C

**The Positional or Internal Parameter**

The trend of the positional or internal parameter,  $u$ , values as a function of doping concentration at 180 °C and 200 °C, is displayed in the graphs of figure 8 below.

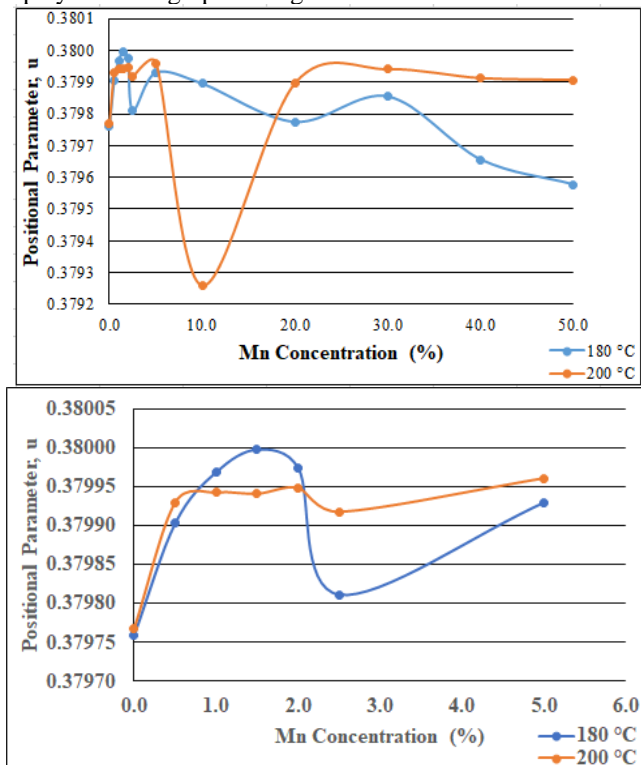


Figure 8: The positional parameter  $u$ , as a function of doping concentration at 180 °C and 200 °C

The positional parameter experimentally observed values from this work was found to be 0.37976 and 0.37977 for temperatures at 180 °C and 200 °C. The values were found to generally increase as the temperature increased from 180 °C to 200 °C. It is only at doping concentration of 10% that the values at 200 °C was found to be far lower than that of 180 °C. The values were observed to either increase or decrease as dopant concentration increase without following any trend at both temperatures. In an ideal wurtzite structure crystal, the internal parameter is given as 0.375 [19]. However, in a real ZnO crystal, the wurtzite structure deviates from the ideal arrangement. The experimentally observed values from this work were found to be higher than the ideal. The deviation from that of the ideal wurtzite crystal is probably due to lattice stability and ionicity [19]. The values of the positional parameter values obtained agree with that reported by Mia et al [18] and Bilgili [22]. The observed fluctuating or irregular trend in the values either increasing or decreasing as dopant concentration increase has also been reported by Senol et al [33].

**Bond Lengths**

The trend of the values of the nearest-neighbor bond lengths along the  $c$ -direction (expressed as  $b$ ) and off  $c$ -axis (expressed as  $b_l$ ) determined using equations 3 and 4 respectively as a function of doping concentration at 180 °C and 200 °C, were found to be irregular as is displayed in the graphs of figures 9 (a and b) respectively. The value for the internal parameter in the  $c$ -direction (expressed as  $b$ ) for both 180 °C and 200 °C was found to be approximately 0.198 nm while that off  $c$ -axis (expressed as  $b_l$ ) was found to be approximately 0.261 nm.

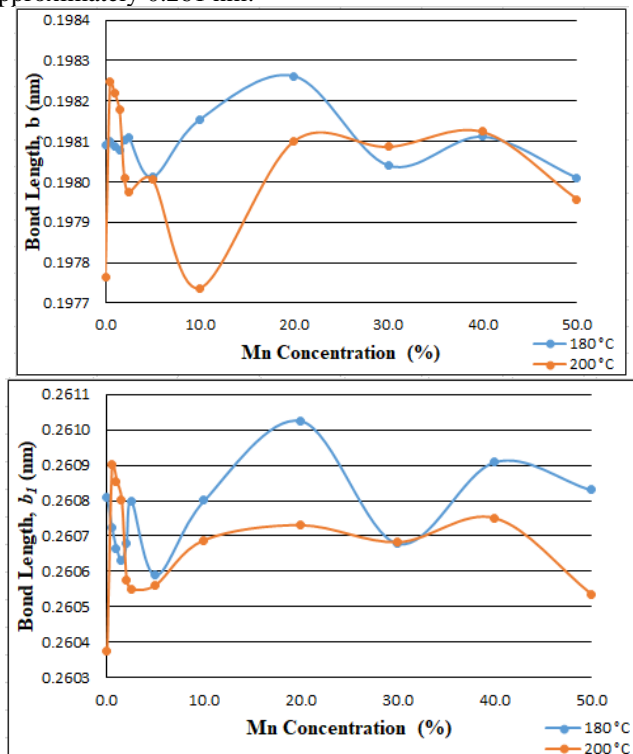


Figure 9: The Bond Lengths  $b$  and  $b_l$  as a function of doping concentration at 180 °C and 200 °C

The nearest-neighbor bond lengths along both the  $c$ -direction ( $b$ ) and off  $c$ -axis ( $b_l$ ) was found to generally decrease as temperature increase from 180 °C to 200 °C. It is only at doping concentration of between 0.5% and 1.5% that the values at 200 °C were found to be higher. However, the values between 0% and 5% follow similar trend. The only difference between the two bond lengths is that, at 10%,  $b$ , recorded the lowest value at 200 °C while  $b_l$  recorded the highest value at 20% for 180 °C.

The fluctuation or irregular trend of the bond length,  $b_l$ , values as a function of doping concentration has been reported by Senol et al [33]. However, the value obtained in this work is in good agreement and in support of the result reported by Mia et al [18] and Nabil et al [20]. Similarly, the values of the  $b$  results couple with irregularity in nature are completely in agreement with preceding research of Mia et al [18]. The variation in the bond length is as a result of the diversity in the peak positions ( $2\theta$ ) along the various planes since both are directly dependent on the lattice parameters  $a$  and  $c$ , and also on the value of  $2\theta$  [13].

### Bond Angles

Using equations 5 and 6 respectively, the bond angles,  $\alpha$  and  $\beta$  for the hexagonal ZnO nanocrystals were observed to either increase or decrease as dopant concentration increase without following any particular trend at both temperatures. The trend of the values as a function of doping concentration at 180 °C and 200 °C, is displayed in the graphs of figures 10 (a and b) below.

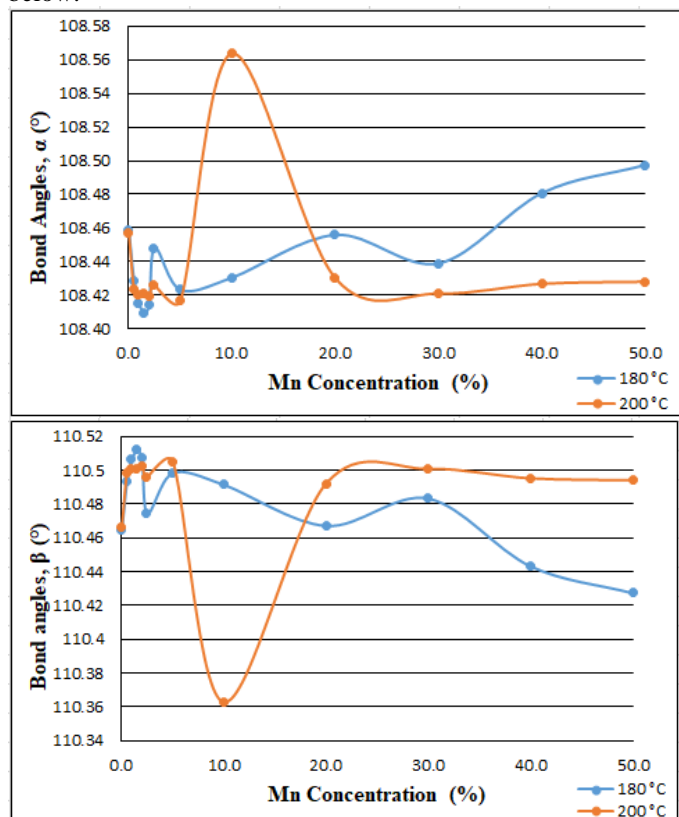


**Figure 10:** The Bond Angles  $\alpha$  and  $\beta$ , as a function of doping concentration at 180 °C and 200 °C

The bond angle  $\alpha$  (Fig 10a), values were found to generally decrease as temperature increase from 180 °C to 200 °C.

Between 0.5% and 2% doping concentration, the values at 180 °C were found to be lower. At 10%, the highest value was recorded at 200 °C. Between 20% and 50% the bond angle  $\alpha$ , values decrease as temperature increases. The bond angle  $\beta$  (Fig 10b), values were found to generally increase as temperature increase from 180 °C to 200 °C. Between 0.5% and 2% doping concentration, the values at 180 °C were found to be higher. At 10%, the lowest value was recorded at 200 °C. Between 20% and 50% the bond angles  $\beta$ , increases as temperature increases. The bond angles,  $\alpha$  and  $\beta$  follow similar trends but in reverse direction. The only difference between the two bond angles is that, at 10%  $\alpha$  recorded the highest value while  $\beta$  recorded the lowest value at 200 °C.

In an ideal wurtzite structure crystal, the bond angles,  $\alpha$  and  $\beta$  is given as 109.47°. However, in a real ZnO crystal, the wurtzite structure deviates from the ideal arrangement [19]. The experimentally observed values from this work were found to be approximately 108.4 for  $\alpha$  and 110.4 for  $\beta$  respectively. Both the  $\alpha$  and the  $\beta$  values were found to be lower and higher than the ideal by about 1° respectively. These values of the results are completely in agreement with research of Sharma and Jha [35].

### Determination of Average Crystallite Size

In this work, Scherer's approach of equation 7 was adopted for the determination of the average crystallite size. The trend of the average crystallite size as a function of doping concentration at temperature of 180 °C and 200 °C are displayed in the graphs of figure 11 below.

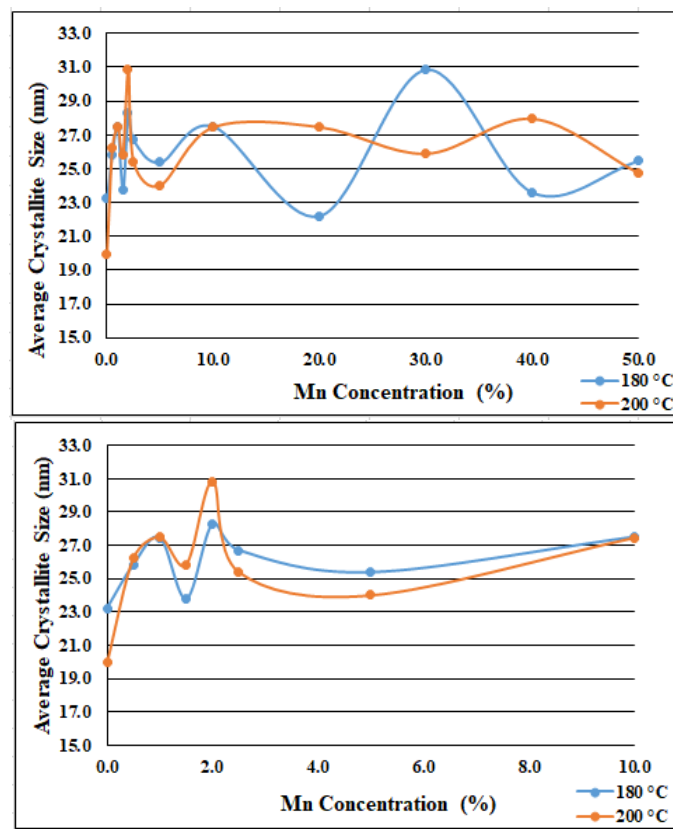


**Figure 11:** The average crystallite size as a function of doping concentration at 180 °C and 200 °C.

At a temperature of 180 °C, the average crystallite size obtained for un-doped ZnO nanoparticles yielded a value of 23.2202 nm and 19.9646 nm for those at 200 °C. For the Mn-doped ZnO nanoparticles at 180 °C, the maximum value is 30.8644 nm at 30% and the minimum value is 22.2035 nm at 20% doping concentration. The average crystallite size at temperature of 200 °C is 30.8417 nm maximum at 2% while the minimum value is 24.0092 nm at 5%. The trend in values shows irregularity in the pattern with the doping concentration. The un-doped ZnO nanoparticles prepared at temperature of 180 °C were found to have bigger crystallite size as compared to the one prepared at 200 °C.

The size of the Mn-doped ZnO nanoparticles were noticed to be irregular (decrease and increase) and not to depend on the concentration of the dopant. At this point it is important to note that, the average crystallite size depends on the diffraction angle (Bragg angle or angular positions of the reflections) which is influenced by structural factors such as the symmetry of the crystals, positions of atoms in the unit cell, the number of electrons of the atoms and the absorption in the material [36]. As a result, the irregular average crystallite size could be attributed to the irregular  $2\theta$  obtained. Similar trend of fluctuating results has been reported by Agarwal et al [6], Abdou and Al-mokhtar [14] and Senol et al [35].

#### Dislocation Density

The dislocation density  $\delta$ , was estimated using equation 8 and the trend of the values as a function of doping concentration at 180 °C and 200 °C, is displayed in the graphs of figure 12 below.

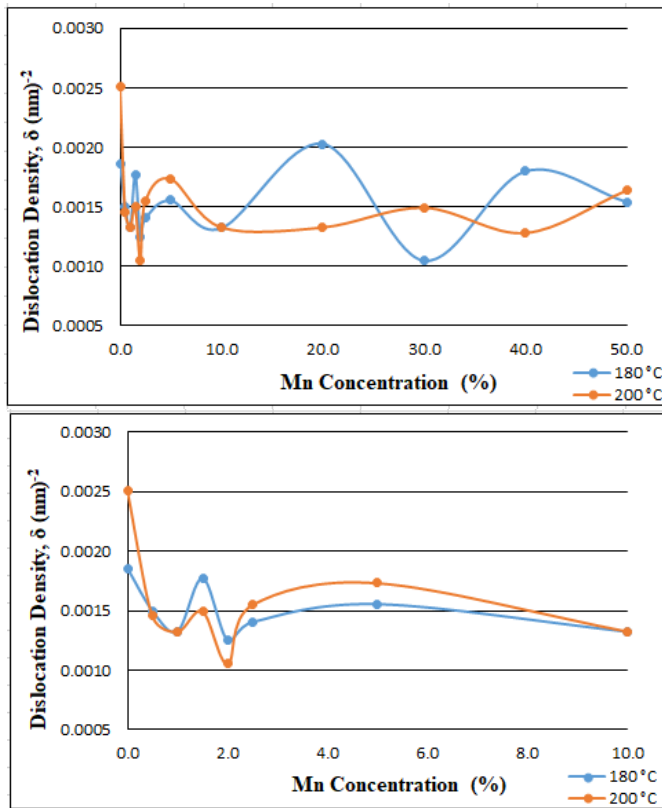


**Figure 12:** The dislocation density as a function of doping concentration at 180 °C and 200 °C.

The dislocation density, representing the extent of defects originating from the internal strain has been found to increase as temperature increases. However, the values were observed to either increase or decrease as dopant concentration increase without following any particular trend at both temperatures. The experimentally observed values from this work were found to be between 0.001050 and 0.002028 (nm)<sup>-2</sup> for 180 °C and 0.001051 and 0.002509 (nm)<sup>-2</sup> for 200 °C respectively. Similar values of this work have been reported by Agarwal et al [6]. The irregular increasing and decreasing trend in values of the dislocation density obtained for this work has been supported by the report of Agarwal et al [6] and Senol et al [33]. A decline in dislocation density specifies reduction in the totality of defects in the crystal growth and vice versa [13]. Additionally, the variation is due to the fact that the dislocation density is inversely proportional to the square of the crystal size which was found to be inconsistent.

#### Lattice Strain

The strain induced in powders due to crystal imperfection and distortion (defects) or atom substitution is calculated using the Wilson formula in equation 9. The trend of the lattice strain as a function of doping concentration at temperature of 180 °C and 200 °C are displayed in the graphs of figure 13 below.

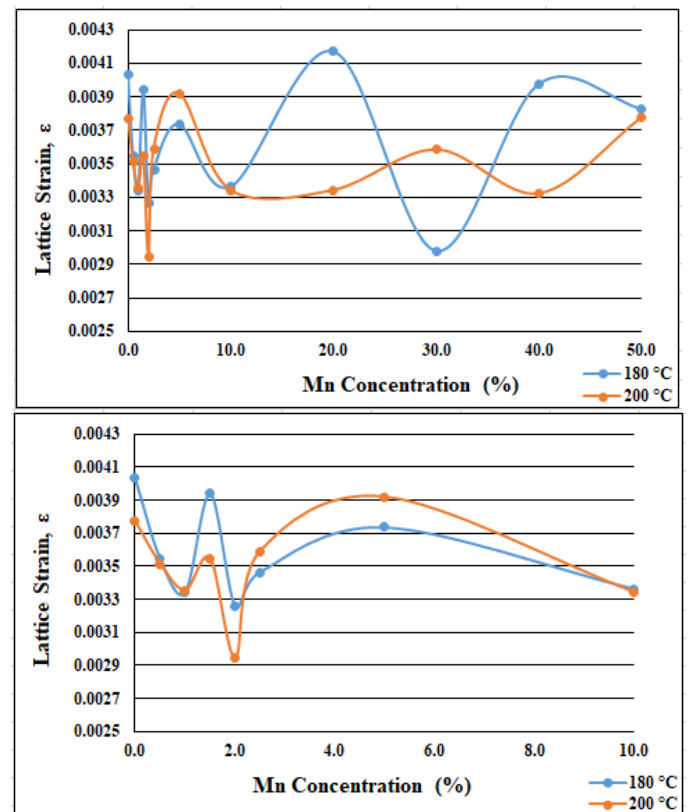


**Figure 13:** The lattice strain  $\epsilon$  as a function of doping concentration at 180 °C and 200 °C.

The strain calculated gives a maximum of 0.00417 at 20% and minimum of 0.002978 at 30% for 180 °C. A maximum of 0.003779 at 50% and minimum of 0.002946 at 2.5% was also calculated at 200 °C. An irregular trend for the values of strain was observed throughout the doping concentrations for both 180 °C and 200 °C. It could be observed that principally,

strain decrease as temperature increases. The values of the lattice strain obtained for this work have been supported by the report of Bilgili [22]. Similarly, the irregular trend in values of the lattice strain has been reported by Agarwal et al [6] and Senol et al [33]. It is known that the more oxygen vacancies are introduced into the crystalline structure, the higher the resulting internal structural strain [37]. A higher value is an indication of more distortion or imperfection while a lower value indicates less imperfection [38].

#### Volume of Unit Cell

The volume of the unit cell was determined using equation 10. Clearly, the volume of unit cell shows both a decrease and an increase in accordance with the fallouts of the lattice parameters for the 180 °C and 200 °C respectively. The minimum was 0.047789 nm<sup>3</sup> at 5% with the maximum as 0.047971 nm<sup>3</sup> at 20% for the 180 °C while the 200 °C recorded minimum of 0.047749 nm<sup>3</sup> at 50% and maximum of 0.04796 nm<sup>3</sup> at 0.5%. According to the ICSD standard data used, the volume of the unit cell is 0.04774 nm<sup>3</sup>. This implies that the values obtain for the work is within acceptable volume of the unit cell of ZnO. A graph relating the volume of unit cell to the dopant concentrations is as shown in figure 14.

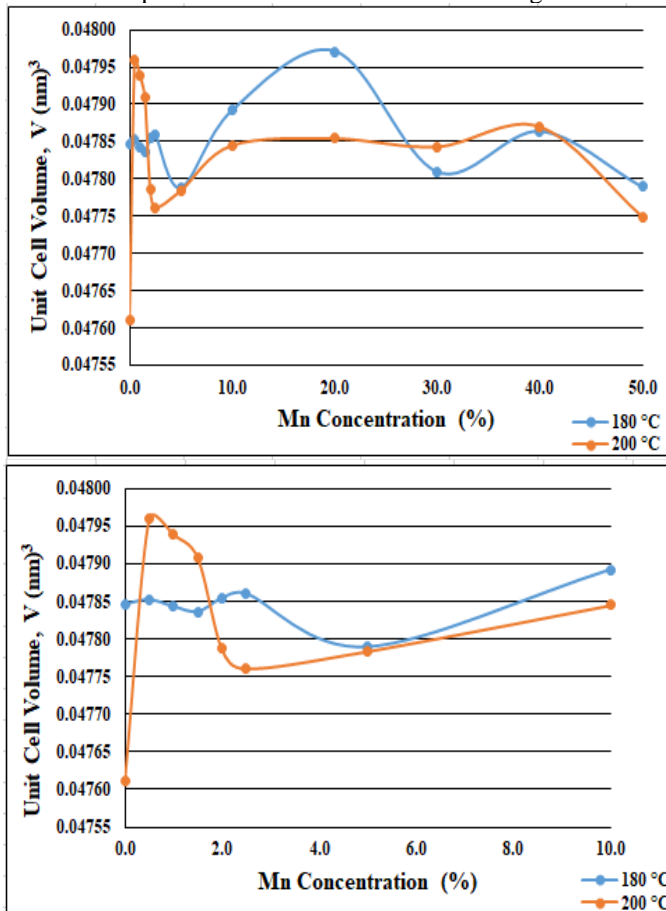


**Figure 14:** The unit cell volume as a function of doping concentration at 180 °C and 200 °C.

The values of the volume of the Mn-doped ZnO samples obtained for this work have been supported by the report of Belkhaoui et al [16] and Nabil et al [20]. Similar irregular trend of the unit cell volume found to be increasing and decreasing as doping concentration increases has been

reported by Agarwal et al [6], Abdou and Al-mokhtar [14] and Senol et al [33]. The irregular trend in the volume of unit cell found with doping concentration may be attributed to the irregular values of the lattice parameters. It indicates that Mn ions have substituted Zn sites available in the structure. Also, the disparity in the volume values is because of the diversity in the peak positions  $2\theta$  along the various planes since both are directly dependent on the lattice parameters [13].

#### Atomic Packing Fraction (APF)

The APF or the parking efficiency is the fraction of volume in a crystal structure that is occupied by constituent particles. This was calculated for the Mn-doped ZnO nanocrystals using the formular in equation 11 and a graph relating the APF to the dopant concentrations is as shown in figure 15.

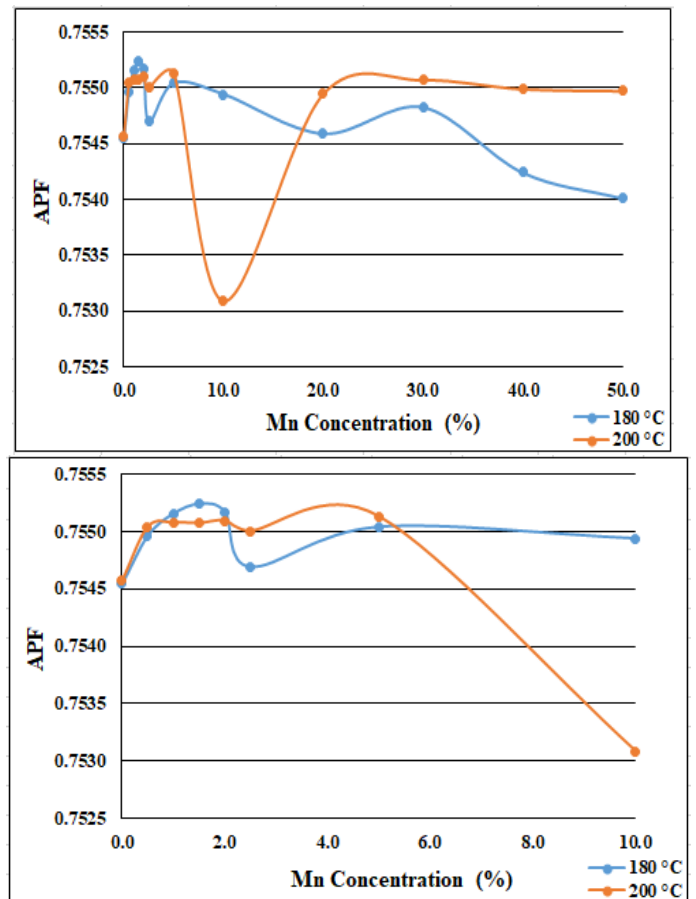


**Figure 15:** The APF as a function of doping concentration at 180 °C and 200 °C.

It can be observed from the graph that, as the dopant is introduced, an irregular trend was observed throughout the doping concentrations for both 180 °C and 200 °C. The APF values obtained for this work is in the range between 0.753 and 0.755 which is approximately 0.75. This irregular trend of the values of the APF found to be increasing and decreasing as doping concentration increases has been reported by Abdou and Al-mokhtar [14] and the value supported by Bilgili [22]. This irregular trend of results possibly will be because of the lattice parameters being the ultimate dependent.

It has been proven that, for an ordered packing of spheres, representing spherical atoms or ions, which is conveniently

used to describe the structure of many crystals upon which the earliest sets of atomic radii were derived, the process must result in equally densest packing of the spheres. At this densest packing of atoms, the fraction of the total volume occupied by the atoms when they touch each other is expected to be approximately 0.74 while the minimum is 0.34 [22][30][39][40].

Thus, the packing efficiency or APF of spheres is 0.74 in the most compact arrangement, which is the highest possible for the packing of equal spheres as in bulk hexagonal ZnO. The values of APF obtained being slightly higher than the bulk is as a result of differences in the ionic radii of the dopant Mn, and the host, Zn. This could be attributed to the fact that most of the substitution might possibly have been achieved by effect of the lower Mn ionic radius being lower than that of the substituted ion of Zn resulting in diminution of empty space in the nanocrystal samples.

### Number of Unit Cell, $n$

The unit cell is the smallest unit of volume that permits identical cells to be stacked together to fill all space was calculated using the formula in equation 12 and the trend as doping concentration increase is irregular. A graph relating the number of unit cell to the dopant concentrations is as shown in figure 16.

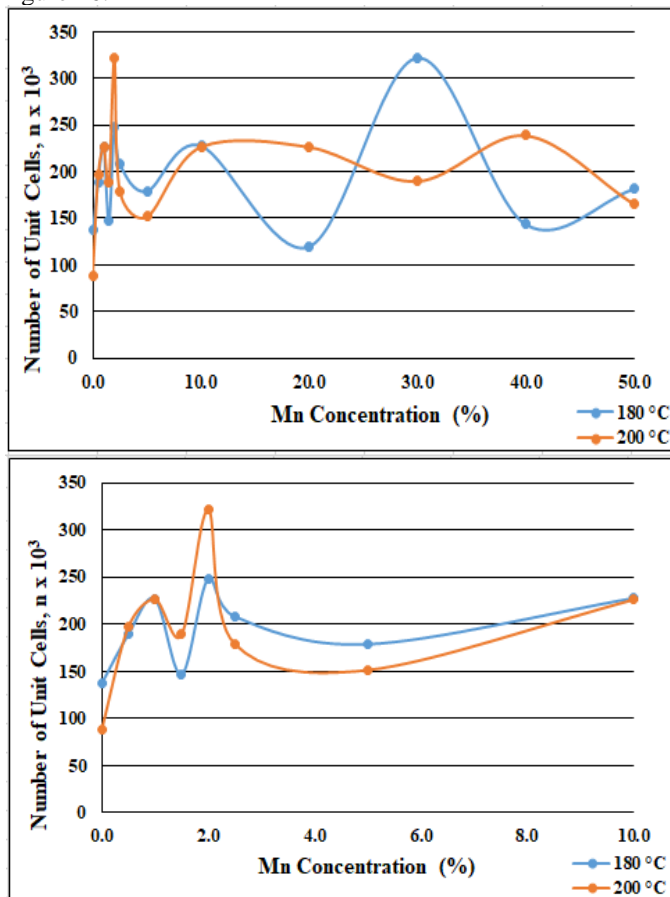


Figure 16: Number of unit cell as a function of doping concentration at 180 °C and 200 °C.

From the graph, it is seen that, when temperature increase for the undoped-doped ZnO, there was a decrease in the number of unit cell. However, when the dopant is introduced, an

irregular trend was observed throughout the doping concentrations for both 180 °C and 200 °C. The values of the number of unit cells realized for this work ranges between 87525 and 322039 with the lowest obtained at 0% doping concentration at synthesis temperature of 200 °C and the highest number of unit cell obtained at 30% doping concentration at synthesis temperature of 180 °C.

### Density

The density of the as prepared samples was calculated using equation 13. The density shows an irregular (decreasing and increasing) trend in accordance with the results of the volume of the unit cell. The minimum density was 5.637 g/cm<sup>3</sup> at 20% for 180 °C with the maximum at 5.664 g/cm<sup>3</sup> at 50% for 200 °C. According to the ICSD standard data used, the density is 5.65 g/cm<sup>3</sup>. This implies that the values obtain for the work is within acceptable density of ZnO. The irregular trend of the density found to be increasing and decreasing as doping concentration increases has been reported by Iqbal et al [41]. The irregular trend may be attributed to the irregular values of the volume of unit cell. A graph relating the density of unit cell to the dopant concentrations is as shown in figure 17.

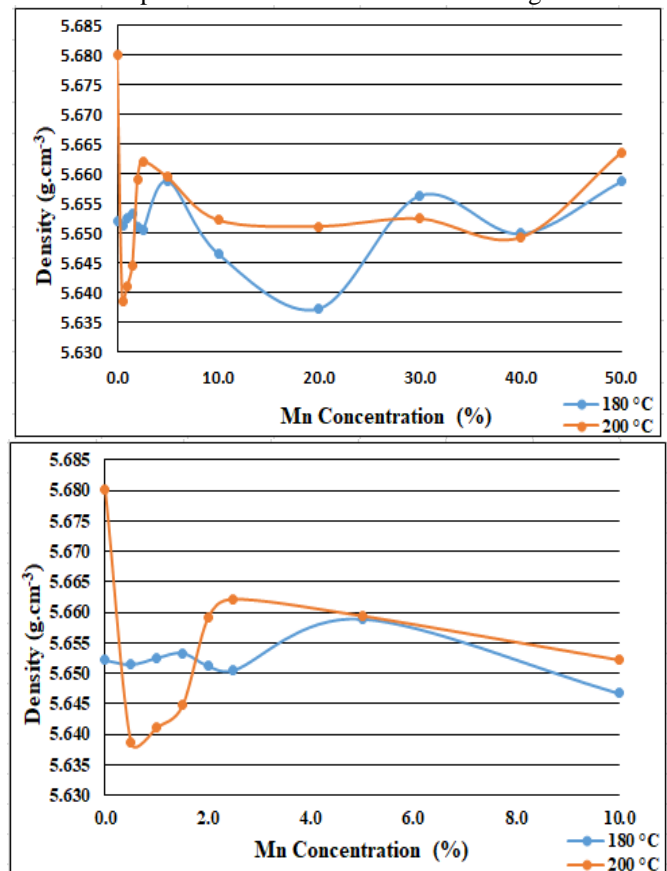
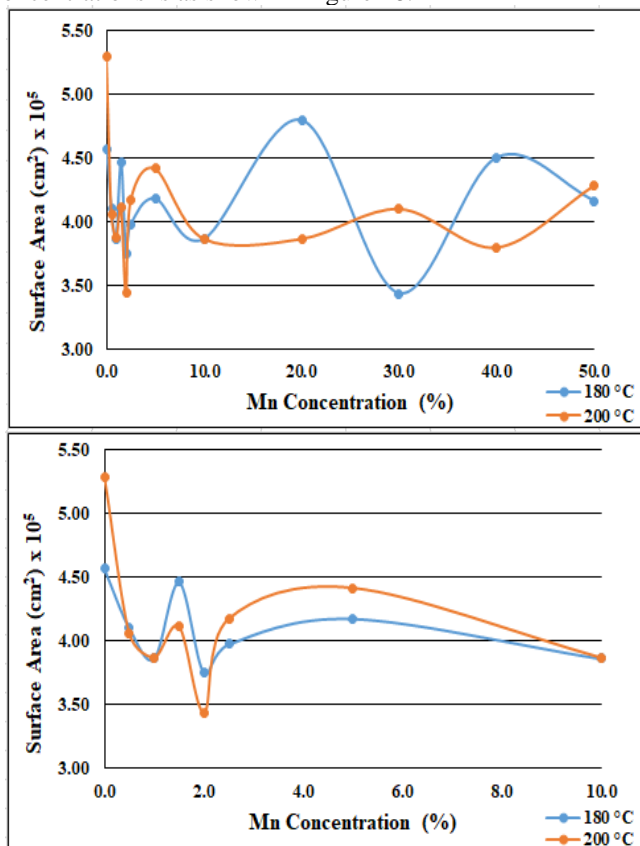


Figure 17: The density as a function of doping concentration at 180 °C and 200 °C.

### Specific Surface Area (SSA)

The SSA of the as prepared samples was calculated using equation 14. An irregular trend in accordance with the results of the density of the unit cell was observed. The SSA for the sample achieved a minimum of  $3.43680 \times 10^5$  cm<sup>2</sup> at 30% and a maximum of  $4.50231 \times 10^5$  cm<sup>2</sup> at 40% both at 180 °C and

200 °C. The results of the SSA are close to those reported by Kaur et al [40]. The irregular trend in the SSA found with doping concentration may be attributed to the irregular values of the density. A graph relating the SSA to the dopant concentrations is as shown in figure 18.



**Figure 18:** The SSA as a function of doping concentration at 180 °C and 200 °C.

## Conclusions

The Mn-doped ZnO nanoparticles with Mn-doping concentrations for the substitution of Zn for  $Zn_{1-x}Mn_xO$  with nominal compositions of  $x = 0.005, 0.01, 0.015, 0.02, 0.025, 0.05, 0.10, 0.15, 0.20, 0.30, 0.40$  and  $0.50$  ( $0 < x \leq 0.5$ ) with corresponding percentage ratios of 0.5%, 1%, 1.5%, 2.5%, 5%, 10%, 20%, 30%, 40% and 50% has been synthesized. The results of the structural characterization including the lattice parameters, bond length, bond angles, crystallite size, strain, volume of unit cell, APF, number of unit cells, specific surface area and the density of the samples were found to be irregular in nature as the doping concentration increases. This variation in the values were due to the irregular values of the interplanar spacing and the observed variations in the shift of the peak angles as a result of the difference in ionic radii between Zn and Mn ions with Mn having multiple ionic radii since all the parameters are directly dependent on the value of the  $2\theta$ .

## References

1. A. Stoklosa. "Molar Volume, Ionic Radii in Stoichiometric and Nonstoichiometric Metal Oxides Stoichiometry and Materials Science - When Numbers Matter", *Innocenti, A. (Ed.)*, ISBN: 978-953-51- 0512-1, InTech, 2012.
2. S. K. Bajpai, V. Thomas and M. Bajpai. "Novel Strategy for Synthesis of ZnO Microparticles Loaded Cotton Fabrics and Investigation of their Antibacterial Properties", *Journal of Engineered Fibers and Fabrics*, 6(3), 2011.
3. S. Sohn and Y. S. Han. "Transparent Conductive Oxide (TCO) Films for Organic Light Emissive Devices (OLEDs), Organic Light Emitting Diode - Material, Process and Devices", Prof. Seung Hwan Ko (Ed.), ISBN: 978-953-307-273-9, InTech, 2011.
4. M. H. Aleinawi, A. U. Ammar, M. Buldu-Akturk, N. S. Turhan, S. Nadupalli and E. Erdem, "Spectroscopic Probing Of Mn-Doped ZnO Nanowires Synthesized via a Microwave-Assisted Route", *J. Phys. Chem. C* 2022, 126, pp. 4229–4240, 2022 <https://doi.org/10.1021/acs.jpcc.2c00009>
5. E. N. A. Armah, F. K. Ampong, M. Egblewogbe, H. A. Koffi, F. Boakye, J. K. A. Amuzu and R. K. Nkum, "Solubility of Mn in ZnO Nanocrystallites using Wet Chemical Synthesis", *Adv. Nan. Res.*; Vol. 2, no. 1, pp: 53-61, November 2019. DOI: <https://doi.org/10.21467/anr.2.1.53-61>
6. M. B. Agarwal, M. Malaidurai, S. Sahoo and R. Thangavel. "Fabrication and Characterization of Mn Doped ZnO Nanoarrays Prepared by Two Step Process", *IP Conference Proceedings* 2327, 020010 (2021) <https://doi.org/10.1063/5.0040024>
7. G. Voicu, O. Oprea, B. S. Vasile and E. Andronescu. "Photoluminescence and Photocatalytic Activity of Mn-Doped ZnO Nanoparticles", *Digest Journal of Nanomaterials and Biostructures*, Vol. 8, No. 2, pp.667-675, 2013.
8. P. Thamaraiselvan, M. Venkatachalam, M. Saroja, P. Gowthaman, S. Ravikumar and S. Shankar, "Structural, morphological, optical and magnetic characterization of Mn Doped ZnO", *International Journal of Multidisciplinary Research and Development*, Vol. 3, No. 3, pp.102-104, 2016.
9. A. R. Babar. "Structural Properties of Mn Doped Zinc Oxide Nanopowders by Chemical Co-Precipitation", *International Journal of Scientific Research in Science and Technology*, Vol. 9, Issue 2, pp. 7-10, April 10, 2021.
10. M. W. Murphy, L. Bovo, G. Bottaro, L. Armelao and T. Sham. "Electronic and relating behavior of Mn doped ZnO nanostructures: An x-ray absorption spectroscopy study", *AIP Advances* 11, 065027, 2021. <https://doi.org/10.1063/5.0047053>
11. Y. Lv, X. Song, T. Lei and P. Yin. "Structural and antibacterial properties of doped zinc oxide and their composites with hydroxyapatite", *Colloids and Surfaces A: Physicochemical and Engineering Aspects*, 651, 129706, 2022. <https://doi.org/10.1016/j.colsurfa.2022.129706>
12. N. A. A. Armah and H. K. Azoda. "Temperature Dependence on Structural Properties of Liquid Phase Synthesized ZnO", *Adv. Nan. Res.*; Vol. 6, Issue 1, pp:11-28, 2023. DOI: <https://doi.org/10.21467/anr.6.1.11-28>
13. A. F. Abdulrahman, S. M. Ahmed, S. M. Hamad and A. A. Barzinjy. "Effect of Growth Temperature on Morphological, Structural, and Optical Properties of ZnO

- Nanorods Using Modified Chemical Bath Deposition Method”, *Journal of Electronic Materials*, Vol. 50, No. 3, 2021. Doi.org/10.1007/s11664-020-08705-7
14. S. M. Abdou and K. M. Al-mokhtar, “Synthesis and Characterization of Mn-Doped ZnO Nanoparticles and Effect of Gamma Radiation”, *Arab J. Nucl. Sci. Appl.*, Vol. 55, no.2, pp.53 -59, 2022.
  15. A. A. Othman, M. A. Osman, E. M. M. Ibrahim, M. A. Ali and A. G. Abd-Elrahim. “Mn-doped ZnO nanocrystals synthesized by sonochemical method: Structural, photoluminescence, and magnetic properties”, *Materials Science and Engineering*, B 219, pp.1–9, 2017.
  16. C. Belkhaoui, N. Mzabi and H. Smaoui. “Investigations on structural, optical and dielectric properties of Mn doped ZnO nanoparticles synthesized by co-precipitation method”, *Materials Research Bulletin 111*, Volume 2021, pp.70–79, 2019. doi.org/10.1155/2021/9926544
  17. H. Morkoc. “Handbook of Nitride Semiconductors and Devices: Materials Properties”, *Physics and Growth*, Vol.1, John Wiley and Sons, New Jersey, 2009.
  18. M. N. H. Mia, S. M. Rana, M. F. Pervez, M. R. Rahman, M. K. Hossain, A. A. Mortuza, M. K. Basher and M. Hoq. “Preparation and spectroscopic analysis of zinc oxide nanorod thin films of different thicknesses”, *Materials Science-Poland*, Vol. 35, no.3, pp.501-510, 2017. DOI: 10.1515/msp-2017-0066
  19. H. Morkoç and Ü. Özgür, “Zinc Oxide: Fundamentals, Materials and Device Technology”, WILEY-VCH Verlag GmbH & Co. KGaA, Weinheim, 2009.
  20. M. Nabil, I. V. Perez-Quintana, M. Acosta, J. A. Mendez-Gamboa and R. Castro-Rodriguez. “Morphological, Structural, and Optical Bandgap Characterization of Extracted ZnO Nanoparticles from Commercial Paste”, *Advances in Materials Science and Engineering*, Volume 2021, pp.1-7, 2021. Doi.org/10.1155/2021/9926544
  21. E. A. Mohammed, “A comparative study of the method of Williamson Hall and the pattern of cadmium oxide nanoparticles for X-rays”, *Turkish Journal of Computer and Mathematics Education* Vol.12, No. 4, pp.881-889, 2021.
  22. O. Bilgili, “The Effects of Mn Doping on the Structural and Optical Properties of ZnO,” *ACTA PHYSICA POLONICA A*, vol. 136, no. 3, pp. 460-465, 2019. DOI: 10.12693/APhysPolA.136.460
  23. R. Kant, D. Sharma, A. Bansal and R. Singh. “Structural, optical and dielectric properties of Al/Mn doped ZnO nanoparticles, a comparative study”, *Materials Technology*, Vol. 36, no.9, pp.513-520, 2021. DOI: 10.1080/10667857.2020.1775408
  24. H. S. Wasly, X-Ray Analysis For Determination The Crystallite Size And Lattice Strain In ZnO Nanoparticles, *Journal of Al Azhar University Engineering Sector*, Vol. 13 No. 49, pp.1312-1320, 2018.
  25. B. Nath and T. F. Barbhuiya, “Studies on the density and surface area of nanoparticles from *Camellia sinensis*, A natural source”, *J. Chem. Pharm. Res.*, Vol. 6, No. 11), pp.08-610, 2014.
  26. A. Zahid, Z. Mukhtar, M. A. Qamar, S. Shahid, S. K. Ali, M. Shariq, H. J. Alathlawi, M. A. Hasan, M. S. Khan, S. Islam, B. R. Patil, M. S. A. Ansari, Z. Nawaz and M. Sher. “Synthesis of Mn-Doped ZnO Nanoparticles and Their Application in the Transesterification of Castor Oil”, *Catalysts* 2023, 13, 105. <https://doi.org/10.3390/catal13010105>
  27. T. M. Dhruvashi and P. K. Shishodia, “Ferromagnetism in sol-gel derived ZnO:Mn nanocrystalline thin films”, *Adv. Mater. Lett.*, vol. 7, no. 2, pp. 116-122, 2016. DOI 10.1007/s13204-012-0089-5
  28. K. P. Bhatti, S. Chaudhary, D. K. Pandya and S. C. Kashyap, *Solid State Commun*; 136:384, 2005.
  29. A. G. Ali, F. B. Dejene, and H. C. Swart, “Effect of Mn doping on the structural and optical properties of sol-gel derived ZnO nanoparticles,” *Cent. Eur. J. Phys.* Vol. 10, No. 2, pp.478-484, 2012.
  30. A. S. Menon, N. Kalarikkal and T. Sabu. “Studies on structural and optical properties of ZnO and Mn-doped ZnO nanopowders”, *Indian Journal of NanoScience*, Vol. 1, No. 2, pp.16-24, 2013.
  31. K. Vasudevan, K. Gopalakrishnan, C. Babu and M. Elango. “Structural and Optical Characterization of Transition Metal Doped ZnO Nanomaterials”, *JIRAS*, Vol. 1, No. 1, pp.98 -104, 2015.
  32. M. Bordbar, S. M. Vasegh, S. Jafari and A. Y. Faal. “Optical and photocatalytic properties undoped and Mn-doped ZnO nanoparticles synthesized by hydrothermal method: Effect of annealing temperature”, *Iranian Journal of Catalysis*, Vol. 5, No. 2, pp.135-141, 2015.
  33. S. D. Senol, E. Ozugurlu and L. Arda, “Synthesis, structure and optical properties of (Mn/Cu) co-doped ZnO nanoparticles”, *Journal of Alloys and Compounds*, 822, pp. 1-12, 2020. DOI: 10.1016/j.jallcom.2019.153514
  34. E. A. Araújo Junior, F. X. Nobre, G. D. S. Sousa, L. S. Cavalcante, M. R. D. M. C. Santos, F. L. Souza and J. M. E. D. Matos. “Synthesis, growth mechanism, optical properties and catalytic activity of ZnO microcrystals obtained via hydrothermal processing”, *RSC Adv.*, Vol.7, 2017. DOI: 10.1039/c7ra03277c
  35. D. Sharma and R. Jha. “Transition metal (Co, Mn) co-doped ZnO nanoparticles: Effect on structural and optical properties”, *Journal of Alloys and Compounds*, 698, pp.532-538, 2017.
  36. M. Ermrich and D. Opper. “X-ray powder diffraction – XRD for the analyst-getting acquainted with the principles”, PANalytical GmbH, Netherlands, 2013.
  37. M. El-Hilo and A. A. Dakhel. “Structural and magnetic properties of Mn-doped ZnO powders”, *Journal of Magnetism and Magnetic Materials*, 323, pp.2202–2205, 2011.
  38. A. H. Moharram, S. A. Mansour, M. A. Hussein and M. Rashad. “Direct Precipitation and Characterization of ZnO Nanoparticles”, *Journal of Nanomaterials*, Vol. 2014, Article ID 716210, 2014.
  39. V. D. Mote, J. S. Dargad and B. N. Dole. “Effect of Mn Doping Concentration on Structural, Morphological and Optical Studies of ZnO Nano-particles”, *Nanoscience and*

- Nanoengineering* 1 (2): pp.116-122, 2013. DOI: 10.13189/nn.2013.010204
40. S. A. Kaur, G. S. Randhawa and R. Singh. "Synthesis and structural analysis of cobalt doped zinc nanoparticles", *IOSR Journal of Applied Physics (IOSR-JAP)*, Volume 9, Issue 5 Ver. III, PP 18-24, Sep. - Oct. 2017. DOI: 10.9790/4861-0905031824
41. T. Iqbal, S. Ghazal, S. Atiq, N. R. Khalid, A. Majid, S. Afsheen and N. A. Niaz, "Influence of Manganese on Structural, Dielectric and Magnetic Properties of ZnO Nanoparticles," *Digest Journal of Nanomaterials and Biostructures*, vol. 11, no. 3, pp. 899-908, September 2016.

